12th International Conference on Electrical, Electronics and Computer Engineering (IcETRAN), Čačak, 9-12 June 2024

# Measurement of the absorption coefficient in an anechoic chamber based on the subtraction method

Marko Janković
*Faculty of Electronic Engineering in Niš,*
*University of Niš,*
Aleksandra Medvedeva 4., 18000 Niš, Serbia
marko.p.jankovic@elfak.rs, 0009-0002-1109-3241

Dejan Ćirić
*Faculty of Electronic Engineering in Niš,*
*University of Niš,*
Aleksandra Medvedeva 4., 18000 Niš, Serbia
dejan.ciric@elfak.ni.ac.rs, 0000-0003-4974-3131

Maro Puljizević
*Kanuf Insulation d.o.o.*
Bodovlje 13, 4220 Škofja Loka, Slovenia
maro.puljizevic@knaufinsulation.com

Aleksandar Pantić
*Knauf Insulation d.o.o.*
Industrijsko naselje Belo polje 4, 17530 Surdulica, Serbia
aleksandar.pantic@knaufinsulation.com

***Abstract* — Persistent inter-laboratory variability in sound absorption coefficient (α) measurements, particularly under the ISO 354 standard, has raised concerns regarding its reproducibility and robustness. This study introduces and critically assesses a modified measurement methodology inspired by ISO 13472-1, adapted for implementation in anechoic environments. The proposed framework incorporates an enhanced measurement configuration and a signal processing strategy based on multi-angular averaging, aimed at improving the stability of measured α and minimizing undesired effects that manifest locally. A comprehensive parametric investigation is conducted to quantify the effects of microphone distance, source location, incidence angle, and sample surface area on α. Experimental results are compared with conventional ISO 354 measurements, the impedance tube method, and numerical simulations based on the Johnson–Champoux–Allard–Lafarge (JCAL) model for rock-mineral wool. The results indicate that the proposed approach yields absorption coefficients that are comparable to those obtained through standardized methods, highlighting its strong potential for adoption as a standardized alternative or complementary technique in acoustic material characterization.**

***Keywords—sound absorption coefficient, subtraction method, anechoic chamber, reverberation chamber, impedance tube***

## I. Introduction

Reliable measurement and calculation of sound absorption properties is essential in architectural acoustics, material engineering, and environmental noise control. Accurate determination of the sound absorption coefficient ($\alpha$) allows for predictive modeling of acoustic environments and supports the design of spaces with optimized auditory performance. As new porous and fibrous materials continue to emerge in the building industry, the need for standardized, reproducible measurement methods becomes increasingly critical for both research and application [1,2].

The most widely accepted methodology for measuring the absorption coefficient is described in ISO 354 [1], which relies on the reverberation time decay in large, diffuse-field reverberation chambers. Despite its long-standing status as the reference method, ISO 354 has been repeatedly criticized for poor inter-laboratory consistency and sensitivity to chamber geometry, source-receiver positioning, and sample mounting conditions [3,4]. Round-robin studies have demonstrated that results for the same material can vary significantly between laboratories, undermining the reliability of the method in comparative or certification contexts (as shown in Fig. 1) [5]. In addition, the impedance tube method (ISO 10534-2) [3], while precise in controlled conditions, suffers from limitations due to sample size, plane-wave assumptions, and edge effects, making it less suitable for characterizing full-scale architectural materials [6]. These methodological shortcomings have prompted ongoing research into more robust and physically consistent alternatives [7].

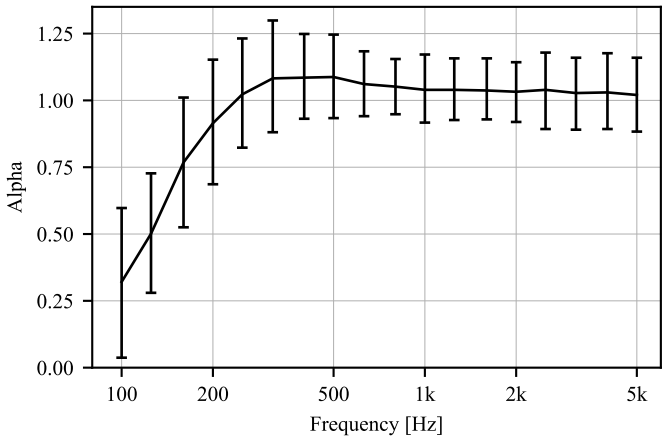


Fig. 1. Mean absorption coefficient of a 100 mm thick mineral wool absorber in a wooden casing with nonwoven fleece, measured across 13 laboratories [5]. Error bars indicate inter-laboratory variability.

In response to the aforementioned limitations, this study introduces an alternative approach to the characterization of sound absorption properties, adapted from the ISO 13472-1 standard [6] and implemented under controlled anechoic conditions. Unlike the original method, which is primarily designed for in situ road surface testing, the proposed procedure features a stationary microphone and a sound source positioned at multiple incidence angles. Key modifications include an expanded measurement geometry and systematic variation of incidence angles. This study explores the effects of changing distance between the sound source and microphone from the test sample, and test material surface, aimed at reducing local anomalies. Additionally, signal processing enhancements are applied to improve measurement repeatability. This framework

This work was supported by the Ministry of Science, Technological Development and Innovation of the Republic of Serbia [grant number 451-03-137/2025-03/200102].

ISBN 978-86-6200-031-6 ©2025 AM & ETRAN
https://doi.org/10.69994/12Ic25002

is intended to yield absorption coefficients with reduced variance and higher inter-laboratory repeatability, while maintaining compatibility with simulation-based benchmarks.

## II. Subtraction Method

The subtraction method for calculating the absorption coefficient involves two consecutive impulse response (IR) measurements using the same measurement configuration (microphone and sound source positions): the first with the material, referred to as the overall IR, and the second without the material, referred to as the reference IR. The overall IR, denoted as $p_m(t)$ in the time domain, is measured at a point close to the test sample surface. This IR consists of the direct $p_i(t)$ sound, and reflected sound $p_r(t)$, coming after a time delay $\tau$ due to the longer travel distance, as well as the unwanted reflections $u$ and extraneous background noise $p_n(t)$ . $K_u$ represents geometric spreading of the unwanted reflections and $r_u(t)$ IR of surfaces that cause unwanted reflections:

$$p_{\mathrm{m}}(t) = p_{\mathrm{i}}(t) + p_r(t) + \sum_u K_u r_u(t) * p_i(t-\tau_u) + p_n(t), \quad (1)$$

where $p_r(t)$ can by expressed as:

$$p_r(t) = K_{\mathrm{r}} r_{\mathrm{p}}(t) * p_{\mathrm{i}}(t-\tau_{\mathrm{r}}). \quad (2)$$

where $r_p(t)$ represents the IR of the surface to be a measured, convolution is denoted by the symbol $*$ and a correction factor $K_{\mathrm{r}}$ is included to account for the geometric spreading of the reflected sound with respect to the incident sound:

$$K_{\mathrm{r}} = \frac{L}{d_s + d_m}, \quad (3)$$

$\tau_{\mathrm{r}}$ is time delay, due to path difference between the direct and reflected sound, and in the case of normal incidence it is:

$$\tau_{\mathrm{r}} = \frac{2d_m}{c}. \quad (4)$$

Fig. 2 illustrates the measurement setup. The parameter $L$ represents the geometrical path length of the direct acoustic wave traveling from the sound source to the microphone. It accounts for the angular displacement of the reflection and is calculated using the law of cosines, considering the distance from the source to the sample ( $d_s$ ), the distance from the microphone to the sample ( $d_m$ ), and the angle of incidence ( $\theta$ ) as described in:

$$L = \sqrt{d_m^2 + d_s^2 - 2d_m d_s \cos(\theta)}. \quad (5)$$

The reflected sound wave (the reflected IR in case of using the IR measurement technique, such as swept sine technique) needs to be separated from the overall sound pressure signal recorded at the microphone. By applying suitable time-domain processing, such as signal subtraction and temporal separation, the reflected IR can be isolated. In that regard, when the reference signal (measured without test sample) is subtracted from the overall signal (measured with test sample), the result will be the reflected sound (the reflected IR):

$$p_r(t) = p_m(t) - p_{ref}(t). \quad (6)$$

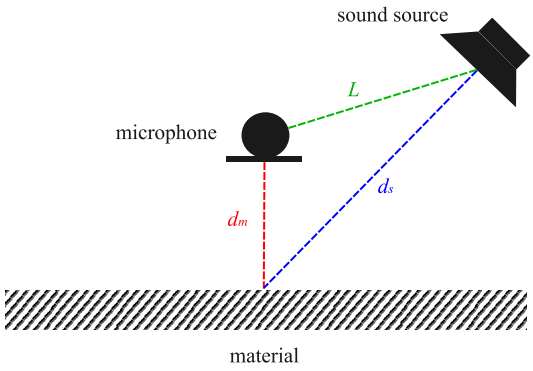


Fig. 2. Geometry of measurement setup.

Under ideal measurement conditions, the subtraction of the reference IR from the overall IR yields only the reflected sound component, as in (6). However, achieving such ideal conditions is extremely challenging due to the presence of parasitic reflections, geometric diffraction effects, and environmental noise that are not entirely eliminated in practical setups [8]. This discrepancy leads to residual components in the subtracted signal that may not accurately represent the true signal reflected from the sample. Consequently, further signal processing techniques, such as synchronization between two IRs (overall and reference) and time-windowing are required to isolate the dominant reflection and suppress secondary artifacts [5]. For this purpose, prior to the subtraction process, two signal synchronization procedures are applied: an initial alignment based on peak-to-peak matching, followed by a fine-tuning algorithm to refine temporal coherence between the overall and reference signals (IRs).

The first synchronization stage, referred to as peak-to-peak alignment, is based on cross-correlation between the two measured signals (two measured IRs) — overall and reference signals. The temporal lag $\Delta t$ that maximizes the cross-correlation function $R_{xy}(\tau)$ is computed as:

$$\Delta t = \arg\max_{\tau} \left[ R_{xy}(\tau) = \sum_n p_{ref}(n) p_m(n+\tau) \right]. \quad (7)$$

where $p_{ref}(n)$ is the reference impulse response and $p_m(n)$ is the overall measured response to be aligned. The signal $p_m(n)$ is then circularly shifted by $\Delta t$ to temporally align its dominant features with those of the reference. This method is robust for aligning transient acoustic signals, particularly in the presence of minor phase deviations or propagation delays [9].

To improve the temporal alignment beyond the sampling resolution achieved by initial cross-correlation, a fine

synchronization step is applied. This process is based on the frequency-domain phase shift method, which enables sub-sample delay correction. The implementation aligns two IRs — overall and reference ones — by minimizing their sum of squared differences (SSD) after applying small fractional phase shifts. The method operates as follows: a representative window is extracted from both IRs (typically near the main peaks,, $p_{mw}(t)$ for overall and $p_{refw}(t)$ for reference IR), the reference IR window is shifted in fine steps via phase manipulation in the frequency domain, where $p_{refw}(t)$ becomes $P_{refw}(\omega)$:

$$\mathrm{P}_{shifted}(\omega) = P_{refw}(\omega) \cdot e^{-j2\pi k \cdot \Delta / N}, \tag{8}$$

where $\Delta \in [-1,1]$ is a fractional delay index tested across a predefined range. For each shift results $\mathrm{P}_{shifted}(\omega)$, the inverse FFT is computed to obtain $p_{shifted}(t)$, and the SSD with the $p_{mw}(t)$ is evaluated as:

$$SSD = \sum_{n} \left[ p_{mw}(t) - p_{shifted}(t) \right]^2 \tag{9}$$

The optimal shift is identified as the one minimizing SSD, and this shift is then applied to the full reference IR.

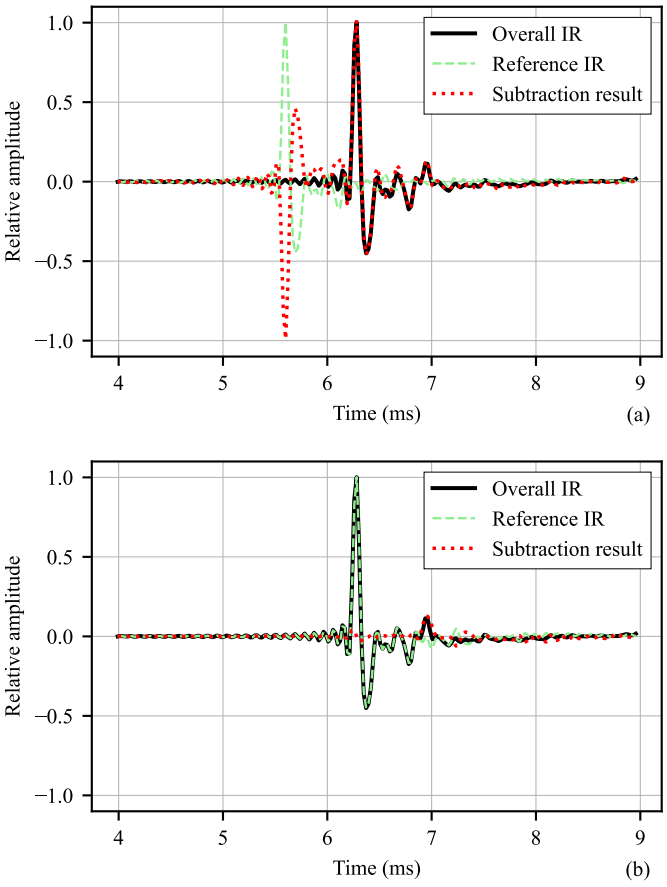


Fig. 3. Results of the subtraction method measured at a 0° angle of incidence, with the sound source positioned 45 cm and the microphone 11.3 cm above the test material: (a) without signal synchronization; (b) after synchronization using peak-to-peak alignment and fine temporal synchronisation.

This method closely follows the principle outlined in [10], which recommends precise time alignment between overall and reference IRs before subtraction. The proposed implementation is a practical realization of this requirement, allowing sub-sample precision without resampling in the time domain. Fig. 3 illustrates the impact of these procedures on the results of the subtraction.

In the next step, time domain IR are transformed into their frequency equivalents by applying the fast Fourier transform (FFT) yielding $P_m(\omega)$ and $P_r(\omega)$. In the frequency domain, $P_m(\omega)$ becomes:

$$P_{\mathrm{m}}(\omega) = P_{\mathrm{i}}(\omega) + P_r(\omega) + \sum_u K_u R_u(\omega) P_{\mathrm{i}}(\omega) \mathrm{e}^{-2\pi i f \tau_u} + P_{\mathrm{n}}(\omega), \tag{10}$$

where the time domain variables from (1) are replaced with their frequency domain counterparts, and $P_r(\omega)$ can be expressed as:

$$P_r(\omega) = K_{\mathrm{r}} R_{\mathrm{p}}(f) P_{\mathrm{i}}(f) \mathrm{e}^{-2\pi i f \tau_{\mathrm{r}}}. \tag{11}$$

In the frequency domain, $p_{ref}(t)$ becomes:

$$P_{\mathrm{ref}}(\omega) = P_{\mathrm{i}}(\omega) + \sum_u K_u R_u(\omega) P_{\mathrm{i}}(\omega) \mathrm{e}^{-2\pi i f \tau_u} + P_{\mathrm{n}}(\omega). \tag{12}$$

By combining the spectra of the $P_r(\omega)$ and $P_{ref}(\omega)$ in the frequency domain, the absorption coefficient can be calculated as follows:

$$\alpha(\omega) = 1 - \frac{1}{K_{\mathrm{r}}^2} \left| \frac{P_{\mathrm{r}}(\omega)}{P_{\mathrm{ref}}(\omega)} \right|^2 \tag{13}$$

## III. Measuremene Setup and Testing Procedure

### A. Measurement environment

All measurements were conducted in the full anechoic chamber of the Faculty of Electronic Engineering, University of Niš, located in Svrljig, Serbia. The chamber is acoustically isolated and designed to simulate free-field conditions by suppressing all reflections across a wide frequency range (from 50 Hz above). The interior is treated with broadband absorbing structures (mainly cubes of different sizes) on the walls, ceiling, and floor boundaries, effectively ensuring that only the direct and sample-reflected sound components reach the microphone. The experimental setup was placed on a suspended wire mesh floor, allowing for precise adjustment of the positions of the loudspeaker and microphone above the test sample without interference from floor reflections.

### B. Equipment and instrumentation

As shown in Fig. 4, a custom-built supporting arc enables angular and distance variation of the sound source and microphone position with high repeatability. The microphone stand allows changing the vertical distance of microphones from the test material, ensuring consistent measurement geometry across all test scenarios. The test (absorbing) material was placed on a rigid plaster-board mounted horizontally over the mesh floor, simulating a reflective boundary beneath the sample. The

absorber was centrally aligned beneath the measurement arc to ensure symmetrical exposure to the incident sound field. The mounting system permitted stable positioning without mechanical contact with surrounding surfaces, minimizing undesired vibrational coupling or edge diffraction artifacts.

The measurement chain was designed to ensure high-fidelity signal acquisition and repeatability. Three Behringer ECM8000 measurement microphones, known for their omnidirectional response and linear frequency characteristic, were used to capture the acoustic pressure signal. As a sound source, Gallo A'DIVA spherical loudspeaker was employed to minimize diffraction effects and ensure a near-point-source radiation pattern. The signals were routed through Zoom F4 field audio recorder, serving as both the audio interface and preamplifier, providing high dynamic range and low noise floor performance. Lenovo Legion laptop computer was used to control signal playback and recording.

For signal acquisition, Adobe Audition was utilized, enabling precise control over the swept sine signal reproduction and synchronized capture of responses. All post-processing — including synchronization, subtraction, time-windowing, and absorption coefficient computation — was performed using custom Python scripts developed for this study.

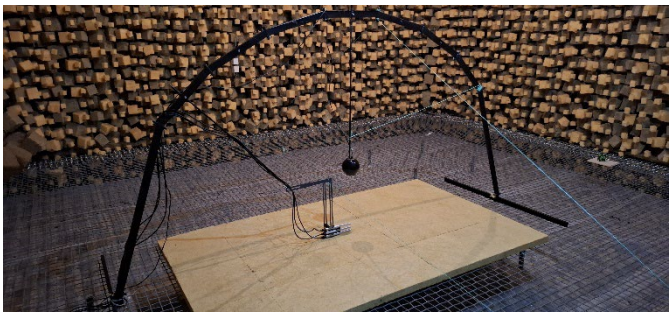

Fig. 4. Measurement hardware setup in anechoic chamber.

### C. Sample configuration

The material under investigation was a 50 mm thick slab of rock wool, by Knauf Insulation. All samples were placed in the horizontal position, resting on a 12.5 mm thick backing plate to ensure consistent reflection conditions and acoustic impedance at the rear boundary. A total of eight different sample sizes were tested to investigate the effect of surface area and edge exposure on the absorption coefficient. The measured configurations included material sizes listed in Table 1:

TABLE I. DIMENSIONS OF MEASURED MATERIAL

| ***Material number*** | ***Size in m²*** |
|---|---|
| 1. | 0.40 × 0.40 |
| 2. | 1.00 × 0.40 |
| 3. | 1.00 × 0.50 |
| 4. | 1.00 × 1.00 |
| 5. | 2.00 × 1.25 |
| 6. | 2.00 × 2.40 |
| 7. | 3.00 × 2.40 |
| 8. | 4.40 × 2.40 |

The presented range of material sizes enabled evaluation of diffraction effects, perimeter-to-area ratio impact, and spatial uniformity in the material's acoustic behavior. Each specimen was carefully centered under the source–receiver arc and flush-mounted to eliminate plate edge discontinuities.

### D. Measurement configuration

To evaluate the influence of spatial and geometric parameters on sound absorption measurement, four distinct measurement configurations were investigated. Each configuration isolated a specific variable, while the remaining parameters were held constant to ensure experimental control and repeatability.

In the first configuration, the distance between the sound source and the surface of the test material was varied to assess the effect of propagation path length on measured absorption. The microphone position was kept fixed at 113 mm above the material surface, and the incidence angle of the source was maintained at 0° (normal incidence). The tested source distances were: 45 cm, 55 cm, 70 cm, 88.5 cm, and 103.5 cm. The material size used in all measurements was 2.00 m × 1.25 m.

In the second set of tests, the distance between the microphone and the test surface was varied, while the sound source remained fixed at a distance of 45 cm and maintained a normal incidence angle (0°). The tested microphone distances, listed in ascending order, were: 1.5 cm, 3.5 cm, 7.5 cm, 8.5 cm, 9.5 cm, 10.5 cm, and 11.3 cm. As before, the material dimensions were 2.00 m × 1.25 m.

The third experiment investigated the effect of changing the source incidence angle on the absorption coefficient. The source was positioned at a fixed distance of 70 cm from the material surface, at several angles of incidence, while the microphone was held constant at 11.3 cm. The tested angles of incidence of the sound source relative to the material's surface normal were: −15°, 0°, 15°, 30°, and 45°. The material sample size remained unchanged at 2.00 m × 1.25 m.

The final configuration explored the effect of test material dimensions on the measured absorption coefficient particularly at lower frequencies where diffraction and edge effects become more prominent. Eight different sizes, as detailed in Table 1, were tested under identical acoustic conditions: source distance of 45 cm at 0° (normal incidence) and microphone distance of 11.3 cm.

## IV. RESULTS AND DISCUSSION

This section presents and discusses the experimental results obtained from the measurement configurations described in Section III, with particular emphasis on the influence of key variables and comparison of the obtained results to those from the reference methods and simulation-based predictions. All plots are presented in one-third-octave bands, in accordance with ISO 13472-1:2022 [4].

Fig. 5 illustrates the variation of the sound absorption coefficient ($\alpha$) as a function of source distance from the material. In the frequency range from 160 Hz to 1 kHz, there is a trend of slight increase of absorption coefficient values with greater source distances. The configuration at 103.5 cm yields higher absorption across this range, particularly between 250 Hz and 1 kHz. This behavior is likely attributed to more favorable wavefront incidence conditions and reduced near-field interference effects when the source is positioned further from

the sample. Within the frequency range from 1 kHz to 10 kHz, spread of the curves is not large meaning that similar values of absorption are obtained, except for 55 cm source distance showing a distinct reduction in absorption centered around 1.6 kHz, deviating notably from the responses of other configurations. In the frequency range between 1.6 kHz and 5 kHz, the difference of the absorption values is below 0.2. The nearly identical absorption coefficient curves regardless of source distance indicate that the measurement becomes increasingly insensitive to source distance variations as the wavelength decreases. These results demonstrate that source distance plays only a certain role in shaping the absorption characteristics at and below 1 kHz, while the effect diminishes at higher frequencies.

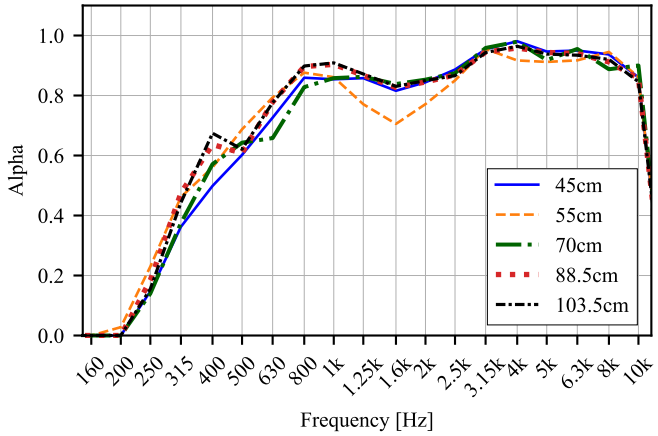


Fig. 5. Effect of source distance from the test sample on the normal incidence absorption coefficient. The sample size was fixed at 2 m × 1.25 m, with a microphone distance of 11.3 cm.

In the frequency range between 160 Hz and 400 Hz, a notable divergence is observed across different microphone distances, Fig. 6. The shortest distances (1.5 cm and 3.5 cm) show significantly elevated absorption values compared to the other configurations. This behavior is not replicated by the other microphone distances, which exhibit a more gradual and comparable rise in absorption with frequency. Between 400 Hz and 5 kHz, most curves display consistent and converging behavior, suggesting stable and reliable absorption measurements across microphone distances. An exception is again the curve for the microphone distance of 1.5 cm, which diverges from the cluster, reflecting measurement instability likely due to spatial interference. Above 5 kHz, absorption curves maintain high consistency across most configurations, confirming robustness in this frequency range. At some frequencies, a single curve — or a few of them — shows significant deviation from the majority of the other curves. This is the case for the curve corresponding to a microphone distance of 7.5 cm at 5 kHz, the curves for distances of 1.5 cm and 3.5 cm at 2 kHz, and the curve for a distance of 11,3 cm at 1.6 kHz. This behavior could potentially be caused by localized reflections or setup variability at those specific distances.

Considering the effects of changing the sound incidence angle, the absorption curves exhibit moderate variability in the frequency range from 160 Hz to 1.25 kHz. This is particularly the case at lower frequencies, where the curves remain tightly grouped, showing a similar rising trend. Only the curve corresponding to an angle of −15° slightly overperforms and underperforms at 400 Hz and 500 Hz, respectively. The 0° curve also follows a comparable path, but sits just below the −15° configuration in the 250–500 Hz region. Between 1.25 kHz and 4 kHz, all curves show certain fluctuations having mainly values between 0.8 and 1. Positions of peaks and dips for different incidence angles are also different. Above 4 kHz, consistency across all angles is generally preserved. The 45° curve has a more prominent peak at 1.6 kHz and more prominent dip at 2.5 kHz, while the −15° configuration slightly drops off after 4 kHz.

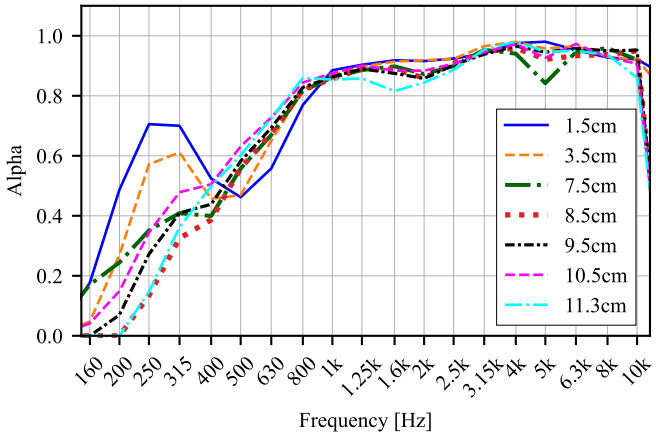


Fig. 6. Effect of microphone distance from the test sample on the normal incidence absorption coefficient. The sample size was fixed at 2 m × 1.25 m, with a sound source distance of 45 cm.

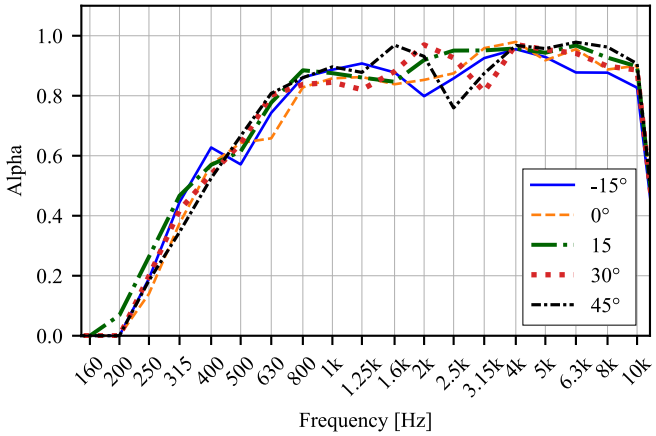


Fig. 7. Effect of different angle of incidence on the absorption coefficient. The sample size was fixed at 2 m × 1.25 m, with a microphone distance of 11.3 cm, and sound source distance of 45 cm.

Analyzing the effects of test sample size, significant variation is observed among the samples in the 160–630 Hz range, with the smallest configuration (0.40 m × 0.40 m) showing higher absorption compared to larger samples. This suggests that absorption performance depends on surface area and perimeter diffraction in this low-frequency region. Between 800 Hz and 3.15 kHz, the absorption curves show exhibit noticeable fluctuations, which grow more pronounced as the test-sample size decreases. Above 3.15 kHz, the absorption curves converge, with differences in absorption coefficients between sample sizes generally less than 0.2. These smaller differences across samples indicate reduced sensitivity to sample size in this frequency range. The observed convergence of the absorption curves confirms that the influence of test surface area and edge effects

diminishes at higher frequencies, where wavelengths are significantly shorter than the sample dimensions.

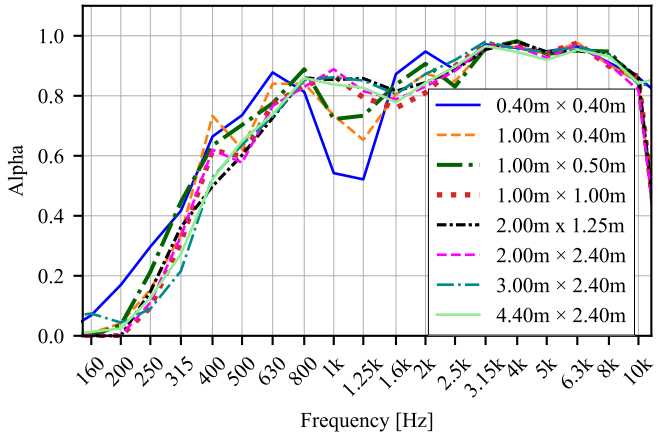


Fig. 8. Effect of different test material sizes on the normal incidence absorption coefficient. The sound source was positioned at 45 cm and the microphone was placed at 11.3 cm.

A strong agreement is observed among the absorption coefficient results above 315 Hz obtained by the subtraction method (averaging the results for different incidence angles -15°, 0°, 15°, 30° and 45°), the impedance tube method, and numerical simulations based on the Johnson–Champoux–Allard–Lafarge (JCAL) model, as shown in Fig. 9. The subtraction method curve (without averaging for the incidence angle of 0°), while generally consistent, exhibits slight deviations between 1.6 kHz and 2 kHz, likely due to local reflection effects or incidence-specific anomalies. The absorption coefficient values obtained by the reverberation room method (for details of the measurements see [12]) show larger variability across the entire frequency range, especially below 400 Hz and above 2 kHz. This highlights the specific characteristics of diffuse-field environment and inter-laboratory inconsistencies frequently associated with ISO 354 measurements.

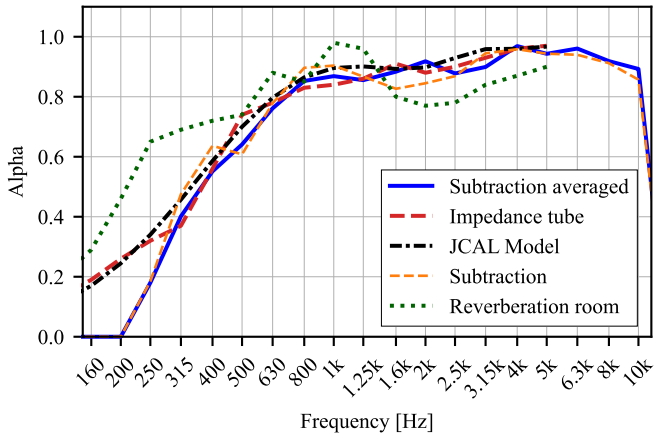


Fig. 9. Comparison of sound absorption coefficients for the same material obtained by using different measurement methods: “Subtraction averaged” by the proposed subtraction method, averaged over five incidence angles as shown in Fig. 7; “Subtraction” by the same method using a single incidence angle of 0°; “Impedance tube” by the measurement in accordance with ISO 10534-2; “Reverberation room” by the measurement conducted in a reverberation chamber according to ISO 354; “JCAL Model” by the numerical simulation based on the JCAL model.

## V. Conclusion and Future Steps

This study presents a measurement approach for evaluating sound absorption coefficient of acoustic materials using a subtraction-based method in an anechoic environment. The investigation of various influencing factors—including source and microphone distance, angle of incidence, and test material size—reveals that the proposed method is sensitive to boundary conditions, especially in lower frequency regions. Still, it produces reliable and repeatable measurements when carefully controlled.

The proposed methodology demonstrates strong agreement with standardized techniques such as the impedance tube method and JCAL simulations, particularly when the results are averaged across multiple incidence angles. Comparative analysis confirms that the subtraction-averaged results show minimal deviation and high consistency across almost entire frequency range, validating the robustness of the approach.

For future work, several directions are proposed to further enhance the methodology of absorption coefficient measurements in anechoic conditions. These include application of other multi-microphone approaches, such as transfer function method, quantification of inter-laboratory variability and estimation of measurement uncertainty, broader validation through testing on acoustically complex and non-flat materials, which present challenges for conventional measurement techniques and automation of the measurement and signal processing chain to improve repeatability and reduce operator dependency. These steps are expected to reinforce the method’s robustness and contribute to the development of future acoustic testing standards.

[1] ISO, *Acoustics — Measurement of sound absorption in a reverberation room*, ISO 354, 2003

[2] J. Balint, M. Berzborn, M. Nolan, and M. Vorländer, “Measuring sound absorption: The hundred-year debate on the reverberation chamber method,” *J. Acoust. Soc. Am.*, vol. 154, no. 4, pp. 2545–2560, 2023.

[3] ISO, *Acoustics — Determination of sound absorption coefficient and impedance in impedance tubes — Part 2: Transfer-function method*, ISO 10534-2, 1998.

[4] ISO, *Acoustics — Measurement of sound absorption properties of road surfaces in situ — Part 1: Noise reduction*, ISO 13472-1:2022.

[5] A. Farina, “Simultaneous Measurement of Impulse Response and Distortion with a Swept-Sine Technique,” in *Preprints of the 108th Convention of the Audio Engineering Society (AES)*, Paris, France, Feb. 2000.

[6] ISO, *Acoustics — Measurement of sound absorption properties of road surfaces in situ — Part 1: Noise reduction*, ISO 13472-1:2022.

[7] A. Farina, “Advancements in Impulse Response Measurements by Sine Sweeps,” in *Proceedings of the 122nd AES Convention*, Vienna, Austria, May 2007.

[8] M. R. Schroeder, “New method of measuring reverberation time,” *J. Acoust. Soc. Am.*, vol. 37, no. 3, pp. 409–412, 1965.

[9] H. Kuttruff, *Room Acoustics*, 6th ed. Boca Raton, FL, USA: CRC Press, 2017.

[10] T. Cox and P. D’Antonio, *Acoustic Absorbers and Diffusers: Theory, Design and Application*, 2nd ed. Boca Raton, FL, USA: CRC Press, 2009.

[11] D. Lafarge, P. Lemarinier, J.-F. Allard, and V. Tarnow, “Dynamic compressibility of air in porous structures at audible frequencies,” *J. Acoust. Soc. Am.*, vol. 102, no. 4, pp. 1995–2006, 1997.

[12] D. Ćirić, M. Puljizević, A. Pantić, and M. Janković, “Energy decay curve deviation in the absorption coefficient measurement in a small reverberation room,” in Proc. Forum Acusticum 2023, Turin, Italy, Sept. 2023, pp. 5591–5598.